1995MNRAS.276..847L

Mon. Not. R. Astron. Soc. **276,** 847–858 (1995)

Growth of perturbations in homogeneous collisionless collapse: discs versus spheres

Walter Landry, Stuart L. Shapiro and Saul A. Teukolsky

Center for Radiophysics and Space Research, and Departments of Astronomy and Physics, Cornell University, Ithaca, New York 14853, USA

Accepted 1995 April 26. Received 1995 March 7; in original form 1994 November 21

ABSTRACT

We study the growth of radial perturbations during the collapse of homogeneous spheres and discs. We model the sphere by concentric shells and the disc by concentric rings, initially at rest and allowed to move only radially. Our numerical experiments show only moderate growth in spheres but rapid growth in discs, leading to pronounced ring formation. For a sphere, the perturbations can be treated analytically as in cosmology. The growth rate is that of a power-law in time and independent of scale. For discs, we present an analytic solution for the perturbations using a suitable mode expansion. Shorter wavelength perturbations grow faster, exhibiting exponential growth at early times.

Key words: instabilities – methods: numerical – galaxies: formation.

1 INTRODUCTION

Contrast the dynamical behaviour of two self-gravitating *equilibrium* configurations of collisionless particles. The first is a homogeneous spherical cluster in which the particles move in randomly oriented circular orbits centred about the origin. The second is a thin disc that one can imagine being formed by squashing the sphere into the equatorial plane, keeping the density homogeneous. Particles in the disc rotate in circles confined to the equatorial plane. The key difference is that the sphere is stable to small perturbations, while the disc is unstable. If we consider only radial perturbations, the sphere is stable because the particles move at all times in the $1/r$ potential of the interior matter, guaranteeing stable orbits. The disc, however, is unstable to the formation of concentric rings (see, e.g., Kalnajs 1972; Fridman & Polyachenko 1984; Binney & Tremaine 1987). Once the matter is perturbed into a ring, the ring potential dominates locally over the potential due to the rest of the matter. Hence the ring attracts more matter and the instability grows. The sphere and disc situations are contrasted in Figs 1 and 2.

Now suppose that the circular velocities of the particles, which are responsible for holding the systems in equilibrium, are set to zero. Both configurations will then collapse radially. In the presence of small radial perturbations, will they behave in the same way as they did in equilibrium? In other words, will the sphere remain stable and collapse homogeneously, and will the disc be unstable to ring formation?

There has been some analytic work on the growth of perturbations in collapsing spheres by Hunter (1962), who performed a hydrodynamic perturbation calculation, including the effects of pressure in a simple way. Unfortunately, the analysis is difficult to carry over to collapsing discs. Instead, we draw an analogy from the well-known behaviour of perturbations in an *expanding* sphere discussed in big bang cosmology. There we know that the evolution of perturbations is described by two modes, one of which grows with time, while the other decays. Both modes are non-exponential, and reduce to power laws in the simplest cases (see, e.g., Peebles 1980). If the situation is time reversed so that the sphere is collapsing instead of expanding, we might expect similar behaviour, that is, essentially power-law growth of linear perturbations. The growth of perturbations during disc collapse does not appear to have been discussed before.

We became interested in these questions in the course of performing numerical calculations of gravitational collapse of finite homogeneous spherical and disc systems in general relativity. There, the collapse of a homogeneous sphere is the simplest example of gravitational collapse, and is described by an analytic solution (Oppenheimer–Snyder collapse; see, e.g., Misner, Thorne & Wheeler 1973). The collapse of a homogeneous disc is the simplest system that can generate gravitational waves from a matter source. Solution of the disc problem requires the full machinery of numerical relativity (Abrahams, Shapiro & Teukolsky 1994). In performing such relativistic simulations in axisymmetry, we observed little tendency for radial perturbations to develop in spherical collapse, but rapid growth of rings during disc collapse. Before assessing this phenomenon in general relativity, we want to clarify the situation in Newtonian gravity.

There have been a number of numerical studies of homogeneous spherical collapse, but most of them are not relevant to the specific issue of pure radial perturbations in collision-

© Royal Astronomical Society • Provided by the NASA Astrophysics Data System

1995MNRAS.276..847L

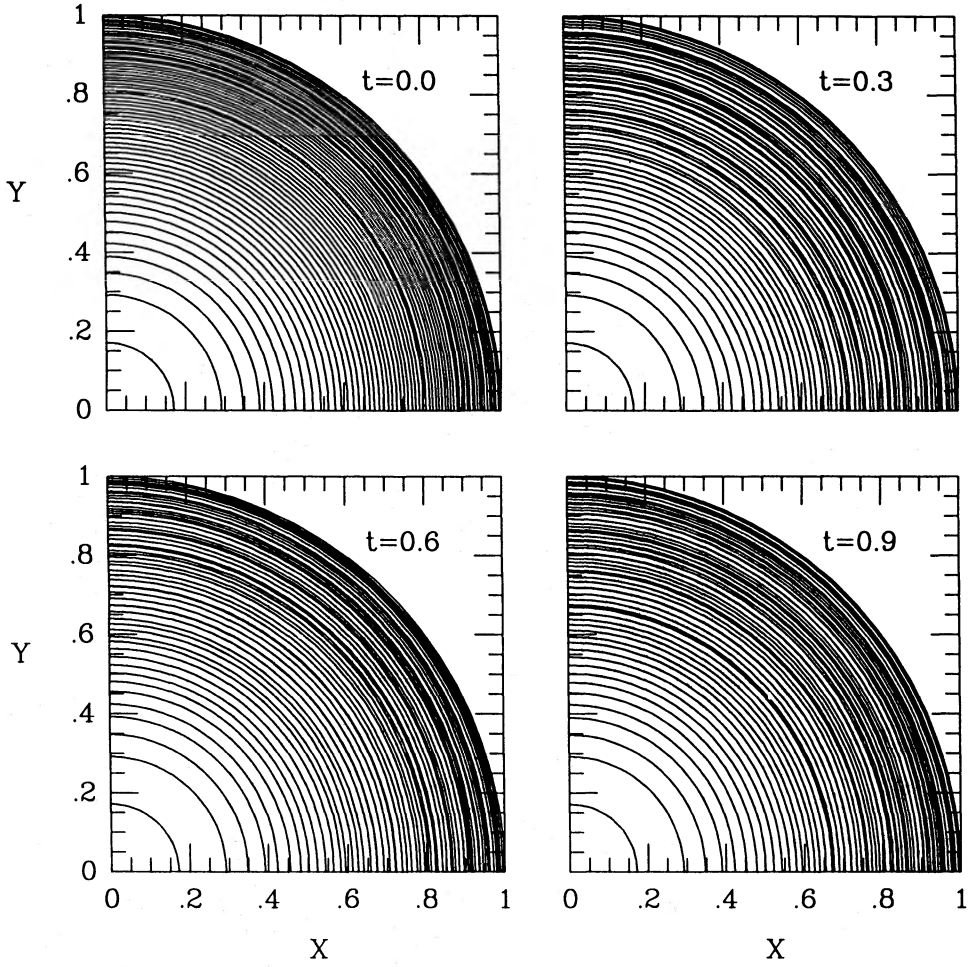

Figure 1. Evolution of spherical shells in an *equilibrium* ($\xi = 1$) sphere slightly perturbed away from homogeneity. The unperturbed shells are distributed so as to give essentially a homogeneous density profile (uniformly in r^3; see Section 3). Small radial perturbations in their positions are introduced as in equation (3.9). The radius of each shell is scaled by the radius of the outermost shell. Time is in units of the orbital period given by equation (2.7). There is no evidence for clumping, and the configuration is stable.

less matter collapse. For example, Henon (1968) is interested in the development of violent relaxation and virialization. Hence the initial conditions contain a distribution of random velocities so that particles do not move only radially. The work by Standish (1968) and Arny & Weismann (1973) uses N-body codes. As a result, discreteness effects induce non-radial motions which ultimately dominate and lead to virialization and violent relaxation. While the effects are certainly interesting for realistic systems, they do not help us understand the specific question we are addressing.

In this paper, we build a simple numerical code to handle spherical and disc collapse of collisionless matter in Newtonian gravity. We take special care to ensure that when unperturbed, the numerical integration scheme preserves homogeneity during collapse. We then assess the growth of radial perturbations when the matter distribution is initially perturbed a small amount away from homogeneity.

We compare our numerical findings with an analytic analysis of linear perturbations. The radial perturbation equation is a partial differential equation in t and r. Since the unperturbed solution describes collapse, the coefficients in the perturbation equation are time-dependent. It is thus not obvious that one can effect a solution by separation of variables. In the case of the sphere, however, separation is possible because not only the unperturbed collapse but also the perturbations themselves evolve homologously. The underlying reason for this is Newton's theorem: the force at a point in a sphere depends only on the total mass interior to that point. Thus a perturbation is not affected. For a disc, by contrast, a local density perturbation changes the gravitational potential at all points of the disc. It is therefore somewhat surprising that the perturbation equation can be separated. We show that expansion of the radial dependence in a suitable set of modes allows such a separation. We find that the resulting equation can be solved analytically for the time dependence of the modes. We use this analytic solution to explain why ring formation in a collapsing disc is much more pronounced than shell formation in a sphere.

2 HOMOGENEOUS COLLAPSE

2.1 Spherical collapse

Consider a homogeneous equilibrium cluster of mass M and radius R_0 consisting of particles moving in randomly oriented circular orbits about the cluster centre. Now

© Royal Astronomical Society • Provided by the NASA Astrophysics Data System

1995MNRAS.276..847L

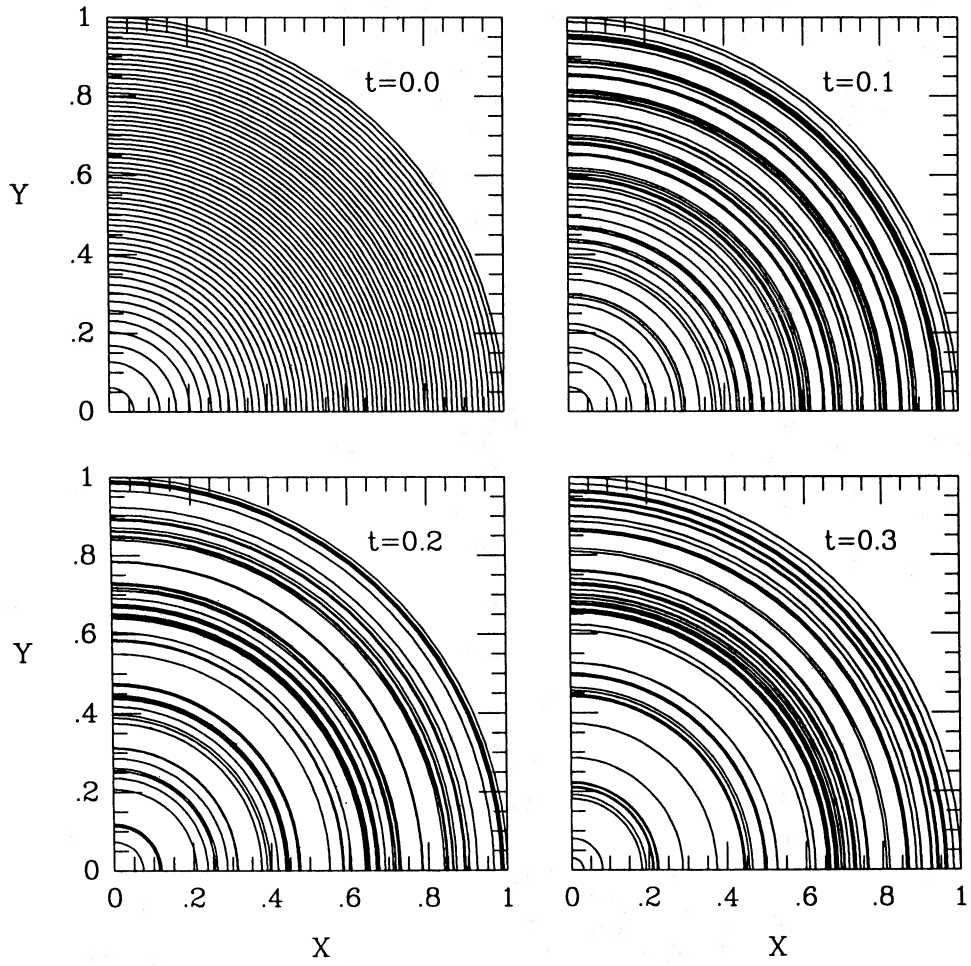

Figure 2. Evolution of rings in an *equilibrium* ($\xi = 1$) disc slightly perturbed away from homogeneity. The unperturbed rings are distributed so as to give essentially the density of a disc formed by squashing a homogeneous sphere into the equatorial plane. Small radial perturbations in their positions are introduced as in equation (3.9). The radius of each ring is scaled by the radius of the outermost ring. Time is in units of the orbital period given by equation (2.7) with $M \to 3\pi M/4$. The perturbations grow rapidly, leading to significant clumping of the rings.

imagine that at $t=0$ all of the velocities are instantaneously reduced by a factor ξ. The resulting evolution consists of a periodic oscillation in which the cluster remains at all times homogeneous. The individual particles move in elliptic orbits with the same period and eccentricity, but with different semimajor axes. (This model was presented in appendix C of Shapiro & Teukolsky 1985, where we used it as a weak-field test of a general relativistic code. See also Shapiro & Teukolsky 1993.) During the evolution, the density of the sphere is given by

$$\rho(t) = \frac{M}{4\pi R^3(t)/3}, \tag{2.1}$$

where $R(t)$ is the radius of the sphere. The interior potential at radius $r \le R$ is

$$\Phi = -\frac{GM}{2R}\left(3 - \frac{r^2}{R^2}\right). \tag{2.2}$$

The equation of motion for R is

$$\ddot{R} = -\frac{GM}{R^2} + \xi^2 \frac{h_0^2}{R^3}. \tag{2.3}$$

Here $h_0 = (GMR_0)^{1/2}$ is the equilibrium angular momentum per unit mass of a particle at the surface. When $\xi = 1$, the sphere is in equilibrium; when $\xi = 0$, the sphere undergoes radial collapse. Set

$$R = R_0 x(t). \tag{2.4}$$

Then the radius r of each particle satisfies

$$r = r_0 x(t), \tag{2.5}$$

where r_0 is the initial radius and $x(t)$ is given by the usual parametric equations for an elliptic orbit:

$$x = a(1 - e\cos u),$$

$$t = \frac{P}{2\pi}(u - e\sin u) - \frac{P}{2}. \tag{2.6}$$

In equation (2.6), the semimajor axis, eccentricity and period are given by

$$a = \frac{1}{2 - \xi^2},$$

$$e = 1 - \xi^2, \tag{2.7}$$

© Royal Astronomical Society • Provided by the NASA Astrophysics Data System

1995MNRAS.276..847L

$$P=2\pi\left[\frac{R_0^3}{GM(2-\xi^2)^3}\right]^{1/2}.$$

Note that the collapse time is given by

$$t_{\rm coll}=\frac{1}{2}P(\xi=0)=\pi\left(\frac{R_0^3}{8GM}\right)^{1/2}. \tag{2.8}$$

The radial and tangential particle velocities are given by

$$v_{\rm r}=\frac{\dot{x}}{x}r,$$
$$v_\phi=\xi\frac{r}{x^2}\left(\frac{GM}{R_0^3}\right)^{1/2}. \tag{2.9}$$

2.2 Disc collapse

Next, consider a disc formed by squashing the above sphere into the equatorial plane while keeping the density homogeneous. The resulting system has a surface density given by

$$\sigma=\frac{3M}{2\pi R^2}\left(1-\frac{r^2}{R^2}\right)^{1/2} \tag{2.10}$$

and an interior potential

$$\Phi=-\frac{3\pi GM}{4R}\left(1-\frac{r^2}{2R^2}\right). \tag{2.11}$$

This is the surface density and potential of a Maclaurin spheroid with eccentricity $e=1$. The evolution of the system is given by the same analytic equations as for the sphere, with the substitution

$$M\rightarrow\frac{3\pi}{4}M \tag{2.12}$$

(Shapiro & Teukolsky 1994). In this case, the collapse time is given by

$$t_{\rm coll}=\frac{1}{2}P(\xi=0)=\pi\left(\frac{R_0^3}{6\pi GM}\right)^{1/2}. \tag{2.13}$$

3 NUMERICAL APPROACH

In constructing a numerical scheme to evolve the collisionless matter, our goal is to minimize the introduction of numerical errors leading to spurious inhomogeneities. Simulation of a continuous homogeneous system using a finite number of elements requires special care. We divide up a sphere into N concentric shells, and a disc into N concentric rings. The force on each element is computed from the difference between the potential at points mid-way to the adjacent elements. The potential at the mid-points is computed by adding up the contributions from each element. In order to preserve the homogeneous profile, at $t=0$ we position the elements at radii such that the potential mid-way between each element is given by the exact analytic value (equations 2.2 and 2.11). Since the analytic potential is quadratic in radius, finite differencing the numerical potential with respect to r^2 will give the exact analytic value of the force on each element, that is, finite difference $\Phi_{,r}$ as $2r\Phi_{,r^2}$. The entire system will then evolve in the same way as a continuous homogeneous configuration, up to the precision with which the equation of motion of each element is solved. Since the equations of motion are ordinary differential equations, they can easily be solved to very high precision. Note that our prescription for evaluating the force on an element by means of a potential automatically incorporates the self-force on an element in a non-singular way.

In the case of an equilibrium configuration ($\xi=1$), we assign to each element a conserved angular momentum

$$h=\xi h_0\left(\frac{r}{R_0}\right)^{1/2}. \tag{3.1}$$

For $\xi=0$, each element has, of course, no angular momentum.

In Section 4 below, we will discuss the subsequnt evolution of an unperturbed distribution of spherical shells or equatorial rings set up according to the above prescription. We will see that the motion reproduces the analytic solution described in Section 2 to any desired accuracy. This gives us confidence that when perturbations are introduced their growth is not due to spurious numerical effects.

3.1 Numerical equations for sphere

The potential at a radius r for N shells at radii r_j, $j=1,\ldots,N$, each of mass $m=M/N$, is

$$\Phi(r)=-Gm\sum_{r_j>r}\frac{1}{r_j}-\frac{GmN_r}{r}, \tag{3.2}$$

where N_r is the number of shells interior to r. At $t=0$, the shell positions r_j are determined by requiring that the potential given by (3.2) above be equal to the analytic potential (2.2) at $r=0$ and the $N-1$ mid-points

$$r_{j+1/2}=\left(\frac{r_j^3+r_{j+1}^3}{2}\right)^{1/3},\qquad j=1,\ldots,N-1. \tag{3.3}$$

The reason that r^3 appears is that in the limit of large N the distribution of shells becomes uniform in r^3. Choosing this prescription therefore gives a good sampling of the density profile. Thus the N equations for the r_j are

$$\Phi(r_{j+1/2})|_{\rm eq.(3.2)}-\Phi(r_{j+1/2})|_{\rm eq.(2.2)}=0,\qquad j=0,\ldots,N-1, \tag{3.4}$$

where we define $r_{1/2}=0$. We solve these equations with a multidimensional Newton's method (Press et al. 1992). The equation of motion for the jth shell is

$$\ddot{r}_j=-\nabla\Phi(r_j)+\frac{h^2}{r_j^3}$$
$$=-2r_j\left[\frac{\Phi(r_{j+1/2})-\Phi(r_{j-1/2})}{r_{j+1/2}^2-r_{j-1/2}^2}\right]+\frac{h^2}{r_j^3}, \tag{3.5}$$

© Royal Astronomical Society • Provided by the NASA Astrophysics Data System

1995MNRAS.276..847L

where we have evaluated the gradient of the potential by finite differencing in r^2 as described above. In equation (3.5), we evaluate $\Phi(r_{N+1/2})$ by quadratic extrapolation in order to give the correct force on the last shell.

3.2 Numerical equations for disc

The potential at equatorial radius r for N rings at radii r_j is

$$\Phi(r) = -\frac{2Gm}{\pi}\sum_j \frac{K(k)}{r_j + r}, \tag{3.6}$$

where K is the complete elliptic integral of the first kind, and

$$k^2 = \frac{4rr_j}{(r_j + r)^2}. \tag{3.7}$$

The procedure for finding the r_j of the rings at $t=0$ is similar to that used for the spherical shells, except that the midpoints are defined by

$$r_{j+1/2} = \left(\frac{r_j^2 + r_{j+1}^2}{2}\right)^{1/2}, \qquad j = 1, \ldots, N-1. \tag{3.8}$$

Here r^2 appears rather than r^3, because the inner portion of the disc is uniformly distributed in r^2 (equation 2.10). The equation of motion for each ring has exactly the same form as equation (3.5).

Note that Φ is logarithmically divergent as $r \to r_j$. However, our prescription for calculating the force yields the same finite value on a ring as in a continuous distribution.

3.3 Perturbations

The point of this analysis is to explore the growth of small radial perturbations in the initial distribution. Accordingly, at $t=0$ we displace each element a fractional amount

$$\frac{\delta r_j}{r_j} = \varepsilon, \tag{3.9}$$

where, for each j, ε is randomly chosen in the interval $(-10^{-3}, 10^{-3})$.

Figs 1 and 2 were obtained by inducing such perturbations. With no perturbations, each frame would be identical to the frame depicted at $t=0$.

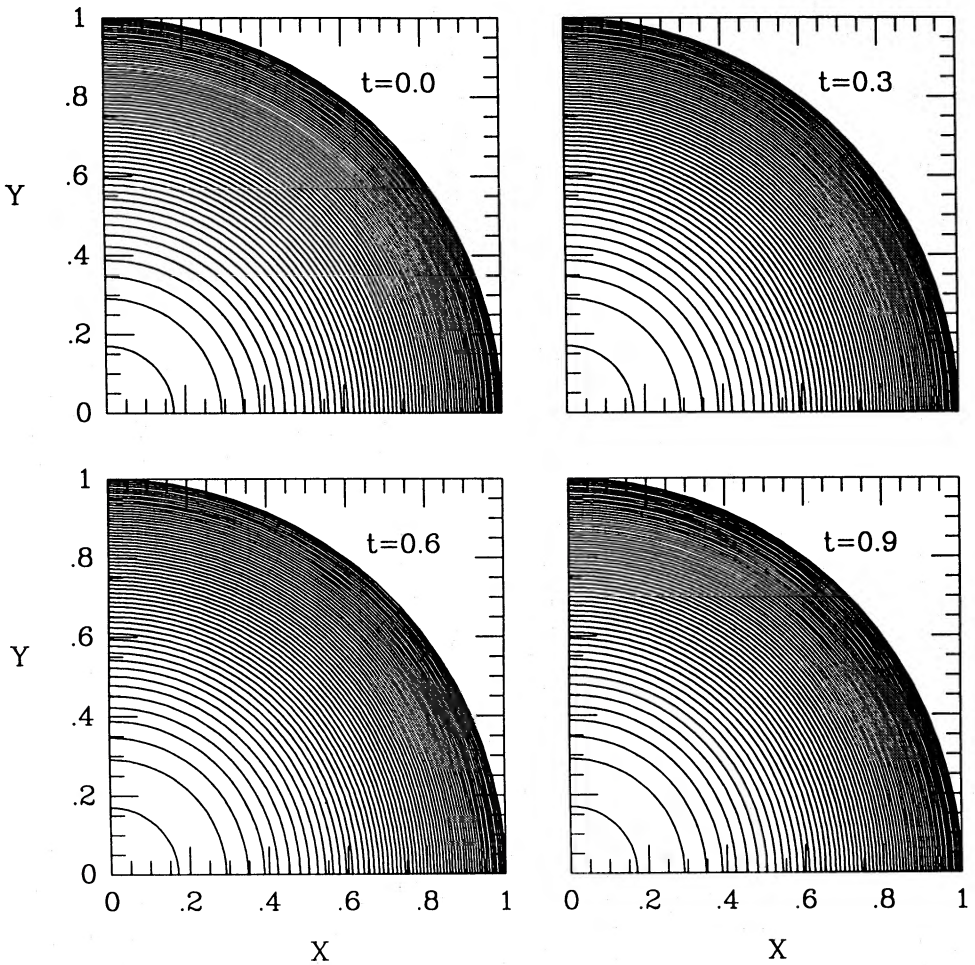

Figure 3. Evolution of spherical shells in a *collapsing* ($\xi = 0$) homogeneous sphere. The shells are distributed so as to give essentially a homogeneous density profile as described in Section 3. The radius of each shell is scaled by the radius of the outermost shell, which has moved in to about 1/3 of its initial value in the last frame shown. Time is in units of the collapse time-scale given by equation (2.8). There is virtually no change in the scaled positions of the shells. To high accuracy, the numerical method introduces no spurious fluctuations and preserves homogeneity.

© Royal Astronomical Society • Provided by the NASA Astrophysics Data System

1995MNRAS.276..847L

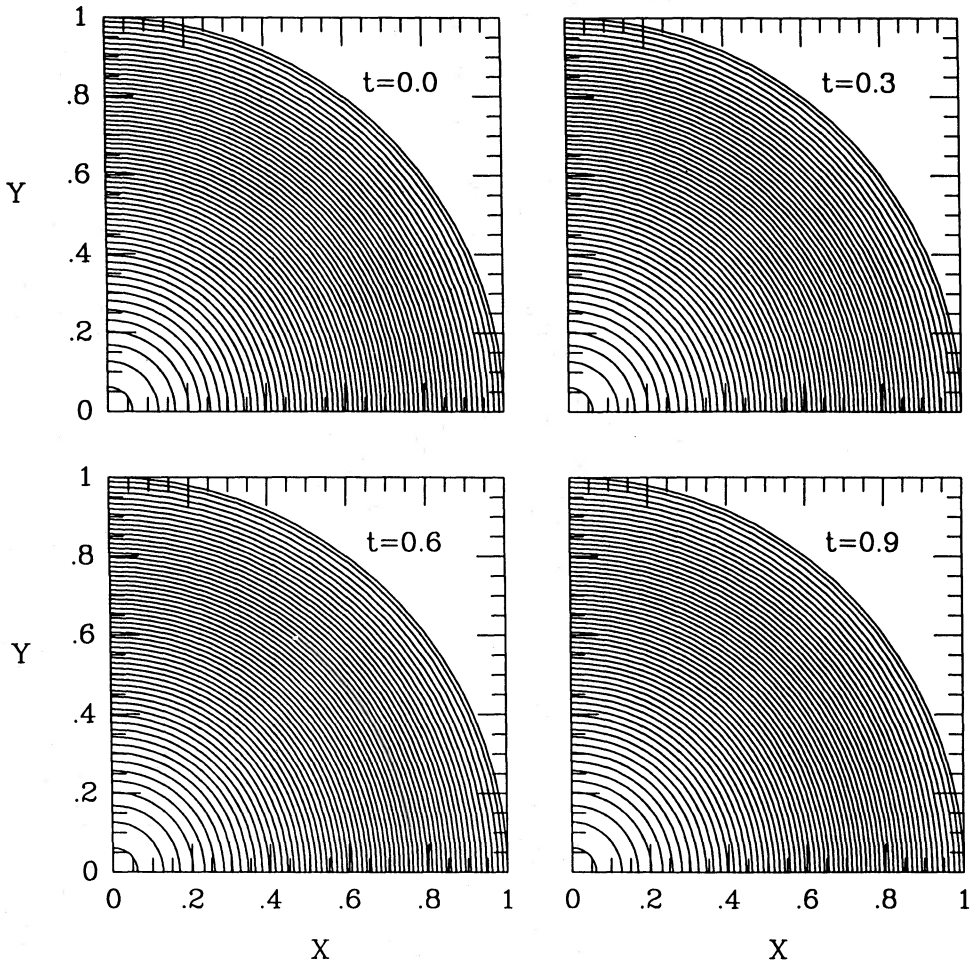

Figure 4. Evolution of rings in a *collapsing* ($\xi = 0$) homogeneous disc. The rings are distributed so as to give essentially the density of a disc formed by squashing a homogeneous sphere into the equatorial plane. The radius of each ring is scaled by the radius of the outermost ring, which has moved in to about 1/3 of its initial value in the last frame shown. Time is in units of the collapse time-scale given by equation (2.13). As for the sphere shown in Fig. 3, there is virtually no change in the scaled positions of the rings. To high accuracy, the numerical method introduces no spurious fluctuations and preserves homogeneity.

3.4 Numerical checks

We have already described one check of the code: reproducing the analytic solutions of Section 2 for unperturbed systems. This applies to collapsing as well as to equilibrium discs and spheres. Total energy conservation provides another check, and it is applicable even when there are perturbations and when those perturbations grow non-linearly.

4 NUMERICAL RESULTS

Figs 3 and 4 show our results for the unperturbed collapse of a homogeneous sphere and disc, respectively. As expected, the collapse is perfectly homologous, and no spurious density fluctuations arise. In these calculations, we used 60 elements. Energy is conserved to better than 3 per cent. Most of the error occurs late in the evolution when the energy is computed as the small difference of large numbers.

Figs 5 and 6 show the results for the same collapse, but with small perturbations introduced at $t = 0$ as described in Section 3. From the figures it is quite evident that the growth of perturbations is much more pronounced in the case of the disc than the sphere. This is similar to the situation we found in Figs 1 and 2 for the perturbed equilibrium configuration.

To quantify this behaviour, we computed a simple correlation statistic to measure the extent to which the elements clump together during collapse. In Fig. 7, we plot, at selected times during the collapse of the sphere, the number of shells $N_<$ whose nearest neighbour is within a volume ΔV. Fig. 8 shows the same plot for disc collapse, but for rings with nearest neighbours within an area ΔA. We see that at $t = 0$ the curves in each plot are both nearly vertical, since the elements are close to being uniformly spaced in volume or area for a homogeneous configuration. At later times, the growth of perturbations is appreciably more rapid for discs than for spheres, as we see from the more rapid rise of the curve at small separations.

© Royal Astronomical Society • Provided by the NASA Astrophysics Data System

1995MNRAS.276..847L

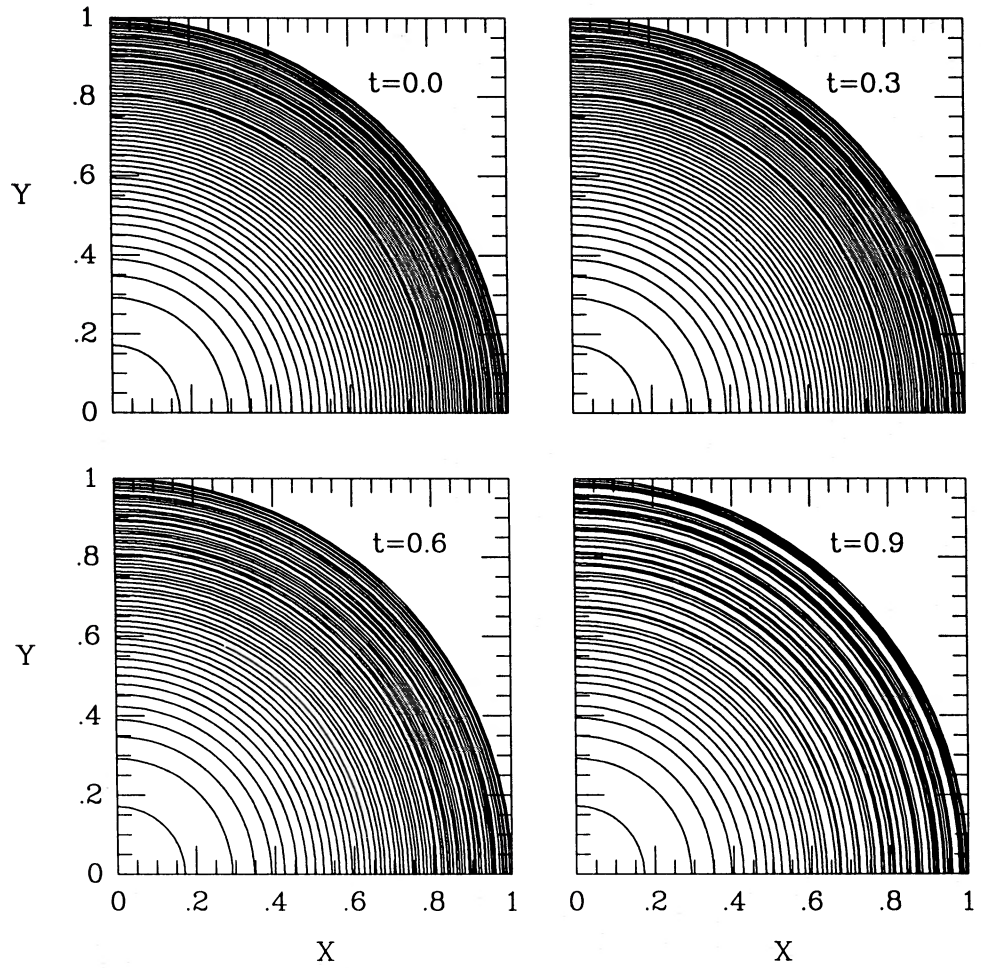

Figure 5. Evolution of spherical shells in the *collapsing* ($\xi = 0$) sphere of Fig. 3, perturbed according to equation (3.9). The perturbations grow very slowly, and are only noticeable toward the end of the collapse.

5 ANALYTIC DERIVATION

To try to understand the observed difference in the growth rates for collapsing homogeneous discs and spheres, we now analyse the growth of perturbations in these configurations analytically. The case of an *expanding* sphere has been treated extensively in the context of cosmology. Here we recast the problem to treat a collapsing sphere. The case of a disc has not been treated before. The key reason why the sphere is so amenable to analytic solution is that the force on a mass shell depends only on the interior mass. Since the force on a ring in a disc is not just a function of the interior mass, it is somewhat unexpected that the disc case can in fact be solved analytically.

The equation of motion for a mass element is

$$\frac{\mathrm{d}\boldsymbol{v}}{\mathrm{d}t} = -\nabla\Phi. \tag{5.1}$$

The change induced by a Lagrangian displacement ξ is governed by the perturbed form of equation (5.1):

$$\Delta\frac{\mathrm{d}\boldsymbol{v}}{\mathrm{d}t} = \frac{\mathrm{d}^2\boldsymbol{\xi}}{\mathrm{d}t^2} = -\Delta\nabla\Phi. \tag{5.2}$$

Note that in the rest of this paper ξ will denote the Lagrangian displacement and not the angular momentum parameter introduced in equation (2.3). Using the identities for Lagrangian perturbations in, for example, section 6.2 of Shapiro & Teukolsky (1983), we get

$$\frac{\mathrm{d}^2\boldsymbol{\xi}}{\mathrm{d}t^2} = -\nabla\delta\Phi - (\boldsymbol{\xi}\cdot\nabla)\nabla\Phi, \tag{5.3}$$

where

$$\delta\Phi = -G\int_V \frac{\delta\rho}{|\boldsymbol{x}-\boldsymbol{x}'|}\,\mathrm{d}^3x' = G\int_V \frac{\nabla'\cdot(\rho'\boldsymbol{\xi}')}{|\boldsymbol{x}-\boldsymbol{x}'|}\,\mathrm{d}^3x'. \tag{5.4}$$

For radial perturbations, equation (5.3) becomes

$$\ddot{\xi} = -\frac{\partial}{\partial r}\delta\Phi - \xi\frac{\partial^2}{\partial r^2}\Phi. \tag{5.5}$$

5.1 Sphere

For radial perturbations of a homogeneous sphere, the gradient of equation (5.4) gives

$$\frac{\partial}{\partial r}\delta\Phi = -\frac{3GM}{R^3}\xi. \tag{5.6}$$

© Royal Astronomical Society • Provided by the NASA Astrophysics Data System

1995MNRAS.276..847L

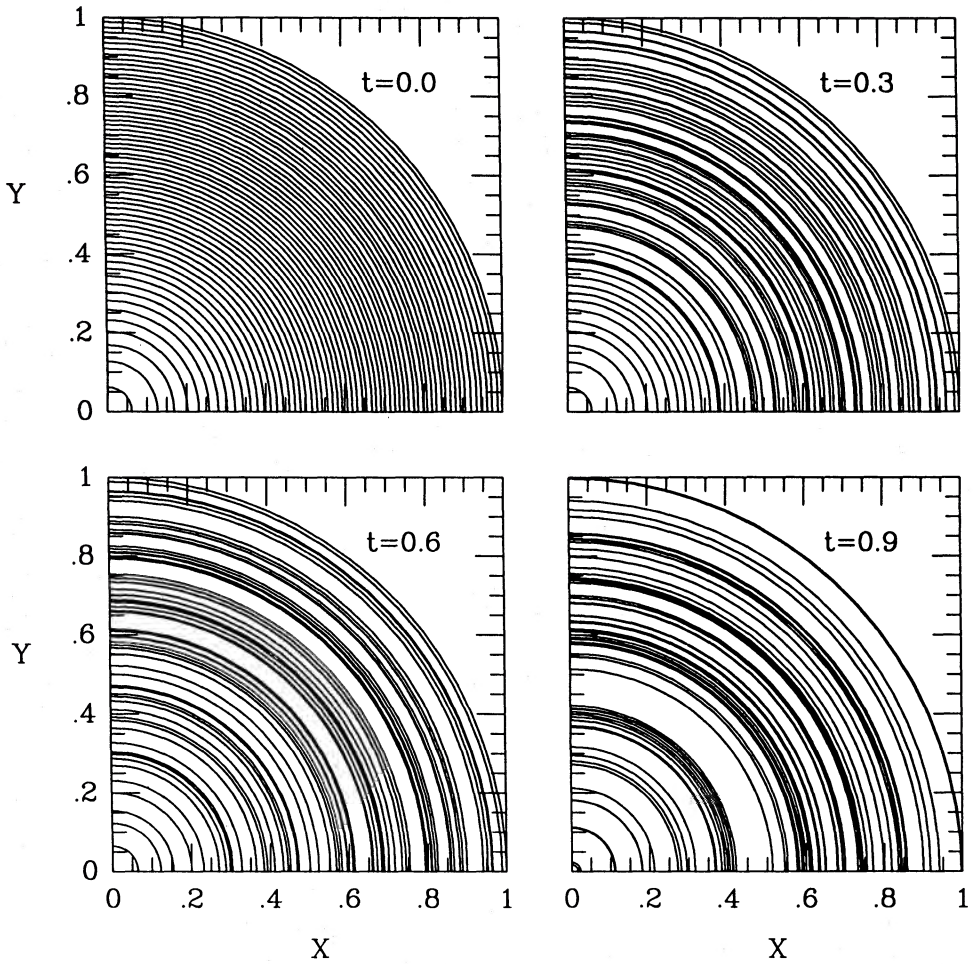

Figure 6. Evolution of rings in the *collapsing* ($\xi = 0$) disc of Fig. 4, perturbed according to equation (3.9). The perturbations grow rapidly, and there is significant clumping of the rings. This is in contrast with the sphere in Fig. 5.

(see, e.g., exercise 6.5 of Shapiro & Teukolsky 1983). The homologous nature of the collapse suggests that we look for a separable solution of the form

$$\frac{\xi}{R} = A(t)\,Z(z), \tag{5.7}$$

where

$$z \equiv r/R. \tag{5.8}$$

Note that, by virtue of equations (2.4) and (2.5), z is independent of time. The left-hand side of the radial perturbation equation (5.5) becomes

$$\ddot{\xi} = \ddot{A}(t)\,RZ(z) + 2\dot{A}(t)\,\dot{R}Z(z) + A(t)\,\ddot{R}Z(z). \tag{5.9}$$

Using equations (2.2) and (2.3), we get

$$\xi \frac{\partial^2}{\partial r^2}\Phi = \xi \frac{GM}{R^3} = -\xi \frac{\ddot{R}}{R}. \tag{5.10}$$

Combining equations (2.8), (5.6), (5.9) and (5.10), equation (5.5) becomes in final form

$$\ddot{A}(t) + 2\dot{A}(t)\frac{\dot{x}}{x} = \frac{3\pi^2}{8t_{\rm coll}^2}\frac{A(t)}{x^2}. \tag{5.11}$$

Note that $Z(z)$ cancelled out: perturbations are independent of scale.

Equation (5.11) is the standard equation for cosmological perturbations with zero pressure (see, e.g., equation 11.1 of Peebles 1980). The two linearly independent solutions (Peebles 1980, equations 11.26 and 11.27) can be written in the form

$$A_1 = -1 + \frac{3}{\sin^2(\eta/2)} - \frac{3}{2}\frac{\eta\cos(\eta/2)}{\sin^3(\eta/2)}, \tag{5.12}$$

$$A_2 = \frac{\cos(\eta/2)}{\sin^3(\eta/2)}. \tag{5.13}$$

For a sphere expanding from zero radius

$$t = \left(\frac{R^3}{8GM}\right)^{1/2}(\eta - \sin\eta) \qquad (0 < \eta < \pi), \tag{5.14}$$

while for a sphere contracting from finite radius

$$t = \left(\frac{R^3}{8GM}\right)^{1/2}(\eta - \pi - \sin\eta) \qquad (\pi < \eta < 2\pi). \tag{5.15}$$

© Royal Astronomical Society • Provided by the NASA Astrophysics Data System

1995MNRAS.276..847L

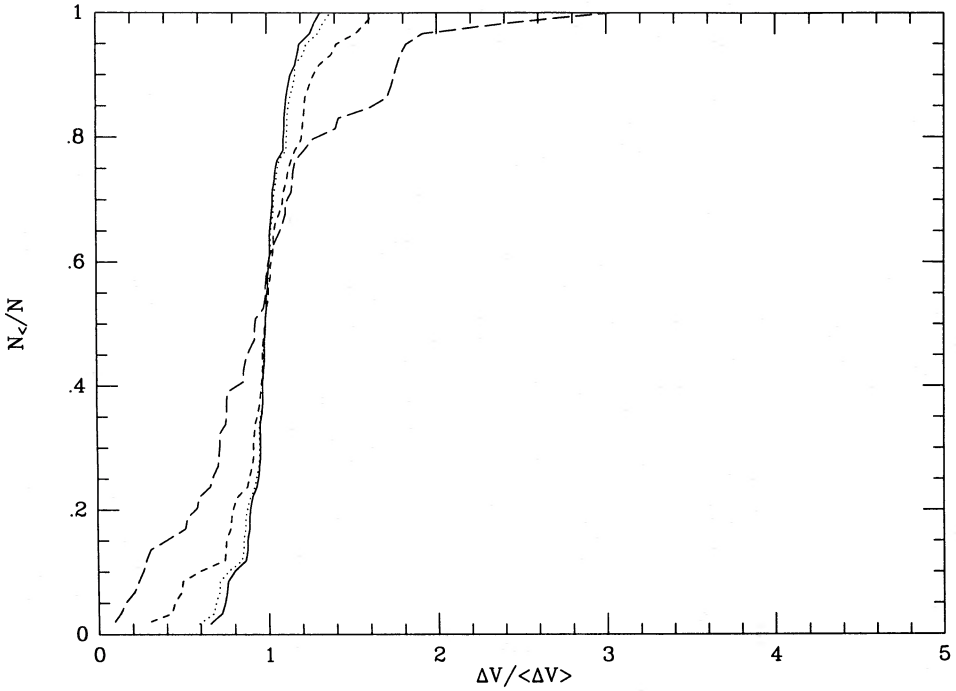

Figure 7. Correlation statistic for the collapsing shells depicted in Fig. 5. We plot the number of shells $N_<$ whose nearest neighbour is within a volume ΔV. The abscissa ΔV is normalized to the mean volume per shell, $\langle \Delta V \rangle = V/N$, where V is the total volume of the sphere. Each curve corresponds to a time shown in Fig. 5: $t=0$ (solid line), $t=0.3$ (dotted line), $t=0.6$ (short-dashed line), and $t=0.9$ (long-dashed line). At $t=0$, the curve is nearly vertical, since the shells are close to being uniformly spaced in volume. At early times (dotted line), there is very little growth of perturbations. At late times, there is a small amount of clumping, as measured by the increase in the number of shells with close nearest neighbours.

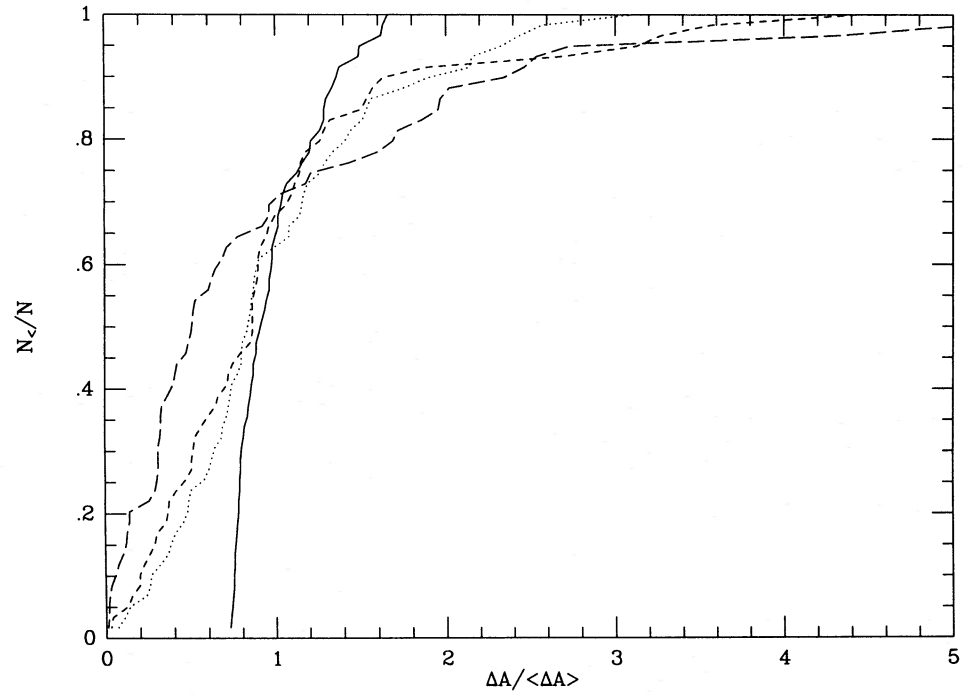

Figure 8. Correlation statistic for the collapsing rings depicted in Fig. 6. We plot the number of rings $N_<$ whose nearest neighbour is within an area ΔA. The abscissa ΔA is normalized to the mean area per ring, $\langle \Delta A \rangle = A/N$, where A is the total area of the disc. Each curve corresponds to a time shown in Fig. 6: $t=0$ (solid line), $t=0.3$ (dotted line), $t=0.6$ (short-dashed line), and $t=0.9$ (long-dashed line). At $t=0$, the curve is nearly vertical, since the rings are close to being uniformly spaced in area. By contrast with the sphere in Fig. 7, even at early times (dotted line) there is substantial growth of perturbations.

© Royal Astronomical Society • Provided by the NASA Astrophysics Data System

1995MNRAS.276..847L

For an expanding sphere, at small t, and hence small η, the solutions reduce to the familiar growing and decaying modes

$$A_1 \sim t^{2/3}, \qquad A_2 \sim t^{-1} \qquad (t \ll t_{\rm coll}). \tag{5.16}$$

For a collapsing sphere, at small t the modes are

$$A_1 \sim 1 + \frac{3\pi^2}{16}\frac{t}{t_{\rm coll}}, \qquad A_2 \sim t \qquad (t \ll t_{\rm coll}). \tag{5.17}$$

This is the case that we have explored numerically in Section 4. The numerical results are consistent with the modest power-law growth of the models in equation (5.17). Eventually, the linear perturbation approximation breaks down: at late times, equations (5.12) and (5.13) predict

$$A_1 \sim A_2 \sim \frac{1}{t - t_{\rm coll}} \qquad (t \to t_{\rm coll}). \tag{5.18}$$

This is in agreement with the result obtained by Hunter (1962) for late times.

5.2 Disc

The analysis of disc perturbations proceeds similarly to that of the sphere. Equation (5.3) remains valid for radial perturbations. Integrating equation (5.4) over the disc thickness, we obtain

$$\delta\Phi = -G\int \frac{\delta\sigma}{|x - x'|}\,{\rm d}^2x'. \tag{5.19}$$

The key difference between perturbations in a disc versus a sphere is that the growth of disc perturbations is not independent of scale. Accordingly, it is necessary to decompose the perturbation into modes and examine the time dependence of each mode separately. Following Kalnajs (1972), who explored the stability of equilibrium discs, we expand the density perturbation in a complete set of functions using Legendre polynomials:

$$\delta\sigma = \sum_{l\,\rm even} \delta\sigma_l = \frac{3M}{2\pi R^2} \sum_{l=2,4,\ldots} b_l(2l+1)\frac{P_l(y)}{y}, \tag{5.20}$$

$$y \equiv \sqrt{1 - z^2}. \tag{5.21}$$

The form of the coefficients in the expansion (5.20) is chosen for later convenience. We will see below that only even l with $l \neq 0$ is allowed in the expansion; otherwise the corresponding Lagrangian displacement would diverge at the edge of the disc.

The Lagrangian displacement is related to the density perturbation by (cf. Shapiro & Teukolsky 1983, equation 6.3.9)

$$\delta\sigma_l = -\nabla\cdot(\sigma\xi_l). \tag{5.22}$$

We integrate both sides of this equation to get

$$\xi_l = -\frac{R}{zy}\int_0^z \frac{P_l(y)}{y}\,z\,{\rm d}z\,b_l(2l+1) = -\frac{b_l R}{zy}[P_{l+1}(y) - P_{l-1}(y)]. \tag{5.23}$$

Here $l = 0$ is excluded for the integral to be finite at $y = 0$.

We again look for a separable solution of the form in equation (5.7)

$$\frac{\xi_l}{R} = A_l(t)\,Z_l(z), \tag{5.24}$$

where now equation (5.23) suggests that we try

$$Z_l(z) = \frac{P_{l+1}(y) - P_{l-1}(y)}{zy}. \tag{5.25}$$

For Z to be regular at $y = 0$, l must be even. For even l, $Z_l(z)$ is regular everywhere; in fact, it is just an odd polynomial in z:

$$Z_l(z) = \frac{P_{l+1}(y) - P_{l-1}(y)}{zy} = \frac{\text{odd polynomial in } y}{zy} = \frac{\text{even polynomial in } z}{z}. \tag{5.26}$$

To find the constant term of this even polynomial, we evaluate it when $z = 0$:

$$\left.\frac{P_{l+1}(y) - P_{l-1}(y)}{y}\right|_{z=0} = \left.\frac{P_{l+1}(y) - P_{l-1}(y)}{y}\right|_{y=1} = 0 + O(z^2). \tag{5.27}$$

Thus $Z_l(z)$ is an odd polynomial in z.

The advantage of using this expansion for the perturbation is that the corresponding potential is expressible in closed form (Kalnajs 1972, equation 8):

$$\delta\Phi_l = -\frac{3\pi GMA_l(t)}{4R}\,p_l P_l(y)\,b_l(2l+1), \tag{5.28}$$

$$p_l \equiv \frac{2}{\pi}\left\{\frac{\Gamma[(l+1)/2]}{\Gamma[l/2+1]}\right\}^2. \tag{5.29}$$

For the radial perturbation equation (5.3), we need the gradient of $\delta\Phi_l$. Using the identity

$$\frac{{\rm d}P_l(x)}{{\rm d}x} = \frac{1}{x^2-1}\frac{l(l+1)}{2l+1}[P_{l+1}(x) - P_{l-1}(x)], \tag{5.30}$$

together with equations (5.21) and (5.24), we obtain

$$\nabla\delta\Phi_l = -\frac{3\pi GMA_l(t)p_l}{4R^2}\frac{b_l l(l+1)}{zy}[P_{l+1}(y) - P_{l-1}(y)] = -\frac{3\pi GM}{4R^3}\,p_l l(l+1)\xi_l.$$

Using equation (5.9) and the analogue of equation (5.10) with $M \to 3\pi M/4$ in the radial perturbation equation (5.3),

© Royal Astronomical Society • Provided by the NASA Astrophysics Data System

1995MNRAS.276..847L

together with equations (5.24) and (5.31), we obtain

$$\ddot{A}_l(t)\,RZ_l(z)+2\dot{A}_l(t)\,\dot{R}Z_l(z)=\frac{3\pi GMA_l(t)\,p_l}{4R^2}\,l(l+1)\,Z_l(z). \tag{5.32}$$

More simply, using equations (2.4) and (2.13), we get

$$\ddot{A}_l+2\frac{\dot{x}}{x}\dot{A}_l=\frac{\pi^2}{8t_{\rm coll}^2}\frac{A_l(t)}{x^3}\,p_l l(l+1). \tag{5.33}$$

We immediately recognize that for the lowest mode $l=2$, the dynamical equation (5.33) is identical to equation (5.11) for a sphere. In the case of a disc, this mode just represents a homologous contraction or expansion. As we found previously, its growth rate is simply a power law in time (equation 5.17). While any perturbation of a sphere behaves in this way, for a disc the higher l modes grow much faster. For large l, the use of Stirling's formula in equation (5.29) yields

$$p_l l(l+1)\rightarrow 4l/\pi. \tag{5.34}$$

Clearly, the driving term on the right-hand side of equation (5.33) grows with increasing l, and hence high-l perturbations will grow faster than low-l perturbations.

To solve equation (5.33) exactly, we first express it solely in terms of $x(t)$ using equation (2.6), (2.7) and (2.13).

$$(1-x)\frac{{\rm d}^2A}{{\rm d}x^2}+\frac{3-4x}{2x}\frac{{\rm d}A}{{\rm d}x}=\frac{w^2A}{x^2}, \tag{5.35}$$

$$w^2\equiv\frac{p_l l(l+1)}{2}. \tag{5.36}$$

This is very similar to the hypergeometric equation:

$$x(1-x)\frac{{\rm d}^2u}{{\rm d}x^2}+[\nu-(\lambda+\mu+1)x]\frac{{\rm d}u}{{\rm d}x}-\lambda\mu u=0. \tag{5.37}$$

If we set $A=x^\gamma B$, where γ is for the moment an arbitrary contant, then equation (5.35) becomes

$$x(1-x)\frac{{\rm d}^2B}{{\rm d}x^2}+[3/2+2\gamma-(2\gamma+2)x]\frac{{\rm d}B}{{\rm d}x}+\left[\frac{1}{x}(\gamma^2+\gamma/2-w^2)-\gamma(\gamma+1)\right]B=0. \tag{5.38}$$

So, if we choose $\gamma^2+\gamma/2-w^2=0$, we have a hypergeometric equation with parameters

$$\lambda=\gamma,\qquad \mu=\gamma+1,\qquad \nu=2\gamma+3/2,$$
$$\gamma=\tfrac{1}{4}(-1\pm\sqrt{1+16w^2}). \tag{5.39}$$

We are interested in the initial growth of the perturbation, when x is close to unity. Hence we choose to write the two independent solutions to the hypergeometric equation as expansions in $(1-x)$ (Abramowitz & Stegun 1964, equations 15.5.5 and 15.5.6):

$$u_{1(1)}={}_2F_1(\lambda,\mu,\lambda+\mu-\nu+1;1-x), \tag{5.40}$$

$$u_{2(1)}=(1-x)^{\nu-\lambda-\mu}{}_2F_1(\nu-\lambda,\nu-\mu,\nu-\lambda-\mu+1;1-x). \tag{5.41}$$

Note that we can take only the positive square root for γ in equation (5.39). Choosing the negative root simply interchanges the solutions (5.40) and (5.41) (Gradsteyn & Ryzhik 1980, equation 9.131.1). Thus the final explicit form for the amplitudes is

$$A_1(l,x)=x^{-1/4+h/4}\,{}_2F_1(-1/4+h/4,\,3/4+h/4,\,1/2;\,1-x), \tag{5.42}$$

$$A_2(l,x)=x^{-1/4+h/4}\sqrt{1-x}\,{}_2F_1(5/4+h/4,\,1/4+h/4,\,3/2;\,1-x), \tag{5.43}$$

$$h\equiv\sqrt{1+16w^2}. \tag{5.44}$$

Figs 9 and 10 show the growth of the displacement $\xi_l(t)$ as a function of l, assuming ${\rm d}\xi/{\rm d}t=0$ initially. In Fig. 9, the initial spectrum of modes is chosen to be the same as the perturbation determined by equation (3.9). In Fig. 10, the initial spectrum is chosen to have a flat distribution. It is clear in both cases that the higher modes grow much more quickly and soon dominate. By contrast, all modes in the sphere behave in the same way as the $l=2$ mode of the disc. Since an arbitrary disc perturbation will include higher l modes, the difference in the growth times is now easily understood.

To quantify this behaviour, we look at the large-l limit of the disc amplitudes. For large l, equations (5.34), (5.36) and (5.39) imply

$$\gamma\sim h/4\sim\sqrt{2l/\pi}. \tag{5.45}$$

Using Gradsteyn & Ryzhik (1980, equations 9.121.9 and 9.121.10), we can rewrite equations (5.42) and (5.43) for large l as

$$A_1(l,x)\sim x^{\sqrt{2l/\pi}}\cosh\sqrt{8l(1-x)/\pi}, \tag{5.46}$$

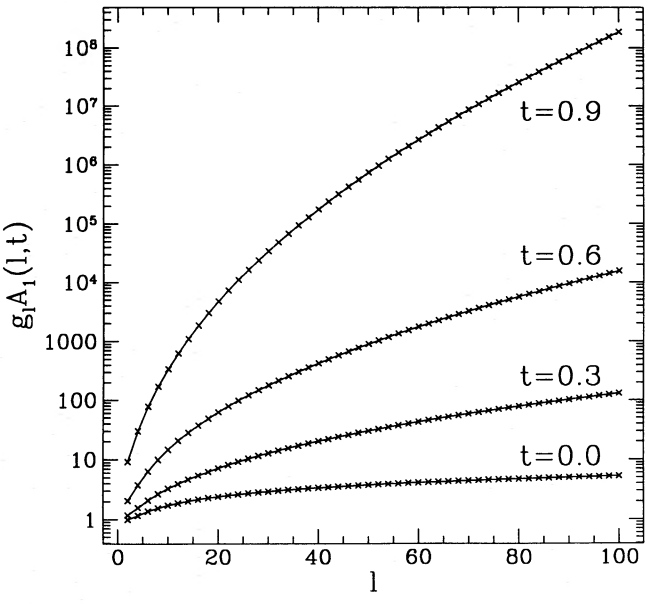

Figure 9. Analytical growth of modes in a collapsing disc. The weighting functions g_l are related to the initial perturbation spectrum prescribed by equation (3.9). They are the rms values of the coefficients that arise when a random spectrum with variance σ^2 is expanded in terms of the functions $Z_l(z)$. They are normalized so that $g_2=1$. For comparison, the only mode present in the sphere is $l=2$. Higher order (shorter wavelength) modes grow much more quickly and soon dominate.

© Royal Astronomical Society • Provided by the NASA Astrophysics Data System

1995MNRAS.276..847L

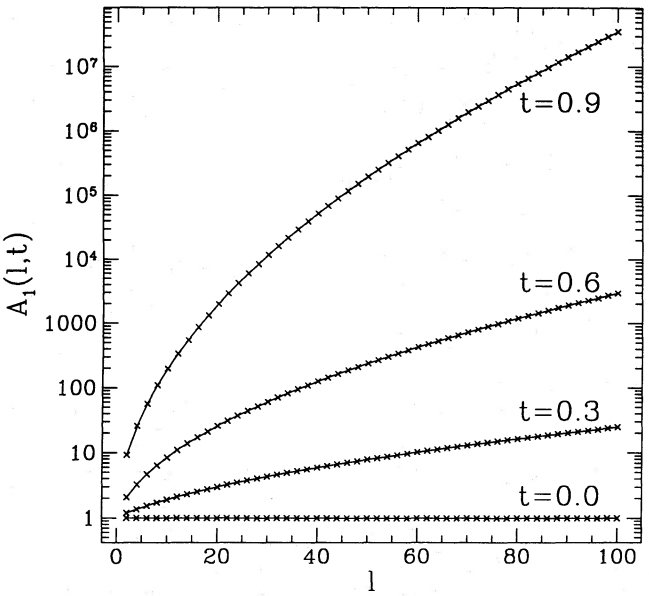

Figure 10. Growth of modes described by equation (5.42). This corresponds to a flat initial spectrum. It is similar to Fig. 9, implying that the result does not depend strongly on the details of the initial perturbation. The highest modes always dominate.

$$A_2(l,x) \sim x^{\sqrt{2l/\pi}} \frac{\sinh\sqrt{8l(1-x)/\pi}}{\sqrt{8l(1-x)/\pi}}. \tag{5.47}$$

At early times, equation (2.6) implies

$$x \sim 1 - \left(\frac{\pi t}{4t_{\rm coll}}\right)^2. \tag{5.48}$$

Therefore, for $\sqrt{l(1-x)} \gg 1$, the solutions become exponentials in time:

$$A_1(l,t) \sim \frac{1}{2}\exp\left(\sqrt{\pi l/2}\,\frac{t}{t_{\rm coll}}\right), \tag{5.49}$$

$$A_2(l,t) \sim \frac{t_{\rm coll}}{t\sqrt{2\pi l}}\exp\left(\sqrt{\pi l/2}\,\frac{t}{t_{\rm coll}}\right). \tag{5.50}$$

Thus, while arbitrary radial perturbations for a collapsing sphere have power-law growth times, disc perturbations have exponential growth times. This accounts for our numerical results. When a homogeneous sphere undergoes gravitational collapse, the slow growth of spherical shells is only discernible at late times. The rapid growth of rings during disc collapse becomes evident almost immediately.

ACKNOWLEDGMENTS

This research was supported in part by NSF grants AST 91-19475 and PHY 94-08378 and NASA grant NAGW-2364 at Cornell University.

REFERENCES

Abrahams A. M., Shapiro S. L., Teukolsky S. A., 1994, Phys. Rev., D, 50, 7282
Abramowitz M., Stegun I. A., eds, 1964, Handbook of Mathematical Functions. National Bureau of Standards, Washington, DC, Section 15.5
Arny T., Weismann P., 1973, AJ, 78, 309
Binney J., Tremaine S., 1987, Galactic Dynamics. Princeton Univ. Press, Princeton, Section 5.3
Fridman A. M., Polyachenko V. L., 1984, Physics of Gravitating Systems. Springer-Verlag, New York, Chapter 4
Gradsteyn I. S., Ryzhik I. M., 1980, Table of Integrals, Series, and Products, Corrected and Enlarged Edition. Academic Press, San Diego
Henon M., 1968, Bull. Astron., 3, 241
Hunter C., 1962, ApJ, 136, 594
Kalnajs A. J., 1972, ApJ, 175, 63
Misner C. W., Thorne K. S., Wheeler J. A., 1973, Gravitation. Freeman, San Francisco, Section 32.4
Peebles P. J. E., 1980, The Large-Scale Structure of the Universe. Princeton Univ. Press, Princeton, Chapter 2, 11
Press W. H., Teukolsky S. A., Vetterling W.T., Flannery B. P., 1992, Numerical Recipes in Fortran: The Art of Scientific Computing, 2nd ed. Cambridge Univ. Press, Cambridge
Shapiro S. L., Teukolsky S. A., 1983, Black Holes, White Dwarfs, and Neutron Stars. Wiley-Interscience, New York, Chapter 6
Shapiro S. L., Teukolsky S. A., 1985, ApJ, 298, 34
Shapiro S. L., Teukolsky S. A., 1993, Phys. Rev. D, 47, 1529
Shapiro S. L., Teukolsky S. A., 1994, Phys. Rev. D, 49, 1886
Standish E. M., 1968, Bull. Astron., 3, 135

© Royal Astronomical Society • Provided by the NASA Astrophysics Data System